Copy 574

[redacted] NASA TM X-54

NASA TM X-54

GROUP (3)
DOWNGRADED AT 12 YEAR
INTERVALS: NOT AUTO-
MATICALLY DECLASSIFIED

TECHNICAL MEMORANDUM

X - 54

INTERACTION OF NONSTEADY TWIN-INLET FLOW AND AIRPLANE DIRECTIONAL MOTIONS AT A MACH NUMBER OF APPROXIMATELY 1.9

By Jack Nugent

High-Speed Flight Station
Edwards, Calif.

FACILITY FORM 602

N71-73436	
(ACCESSION NUMBER)	(THRU)
35	None
(PAGES)	(CODE)
(NASA CR OR TMX OR AD NUMBER)	(CATEGORY)

CATEGORY
SPECIAL HANDLING
7

[redacted]

NATIONAL AERONAUTICS AND SPACE ADMINISTRATION
WASHINGTON October 1959

[redacted]

1Y

[redacted]

NATIONAL AERONAUTICS AND SPACE ADMINISTRATION

TECHNICAL MEMORANDUM X-54

INTERACTION OF NONSTEADY TWIN-INLET FLOW AND AIRPLANE DIRECTIONAL MOTIONS AT A MACH NUMBER OF APPROXIMATELY 1.9*

By Jack Nugent

SUMMARY

Flight tests of a twin-duct propulsion system performed at a Mach number of about 1.9 during nonsteady propulsion-system operation have indicated that an interaction occurred between airplane directional oscillations and fluctuations in an asymmetric shock configuration at the inlets. The airplane directional motion could initiate the asymmetric shock configuration, or, conversely, the asymmetric shock configuration could initiate the airplane directional motion. The asymmetric shock configuration was produced at reduced mass flows and was aggravated by airplane sideslip angle. Initial forward motion of the inlet shock system occurred on the leeward side of the airplane. Installation of a duct splitter plate at the engine face alleviated, but did not eliminate, the interaction phenomenon. The use of a yaw damper was beneficial in reducing directional motions.

INTRODUCTION

Several present-day transonic and supersonic fighter airplanes incorporate the induction system in a twin-duct arrangement in which each duct entrance is mounted at the side of the fuselage. For a single-engine installation this requires that the twin ducts join ahead of the turbojet engine. Such an arrangement must operate in an efficient and stable manner over a range of flight speeds, airplane attitudes, and engine airflow demands; however, wind-tunnel studies of twin-duct installations with a single discharge have shown the existence of a phenomenon known as twin-duct instability (refs. 1 and 2). In this phenomenon there are nonequal flows in the ducts which, for supersonic free-stream Mach numbers, can result in asymmetric shock configurations at the inlet-compression

---

*Title, Unclassified.

[redacted]

surfaces and in directional moments on the fuselage. Furthermore, twin-duct instability is a function of mass flow, flight speed, and airplane attitude (ref. 2).

Tests are being made at the NASA High-Speed Flight Station at Edwards, Calif., on an airplane having an induction system with twin fixed-geometry half-conical inlets and a variable bypass at the duct exit for engine-inlet matching. During the testing program twin-duct instability was encountered inadvertently during roll maneuvers, and undesirable airplane directional motions were produced. To investigate this phenomenon further, additional occurrences of twin-duct instability were obtained intentionally by means of directional maneuvers and abrupt throttle reductions. This paper presents data from three flights obtained during the investigation. Data were obtained at a Mach number of about 1.9 at altitudes ranging from about 42,000 feet to about 46,000 feet.

H118

SYMBOLS

A	area, sq ft
A_c	capture area, both inlets, 763 sq in.
A_{de}	diffuser exit area, 830 sq in. (nominal)
A_{th}	throat area, 543 sq in.
D	distortion parameter, $\Sigma \lvert d \rvert / n$, percent
d	local distortion, $\frac{H_l - H_{de}}{H_{de}}$, percent
H	total pressure, lb/sq ft
H_{cd}	compressor discharge total pressure, lb/sq ft
H_{de}	diffuser-exit total pressure, lb/sq ft
H_0	free-stream total pressure, lb/sq ft
H_{de}/H_0	total pressure recovery
H_l	local total pressure, lb/sq ft

[redacted]

h_p	pressure altitude, ft
M_{de}	diffuser-exit Mach number
M_0	free-stream Mach number
m/m_0	mass-flow ratio, $\frac{(W_e + W_{by})}{\rho_0 A_c V_0}$
N	engine physical speed, rpm
$N/\sqrt{\theta}$	engine corrected speed, rpm
n	number of recording diffuser-exit probes
P	static pressure, lb/sq ft
P_c	static pressure in engine compartment, lb/sq ft
P_{de}	static pressure at diffuser exit, lb/sq ft
P_{de}/H_0	static-pressure recovery
P_0	free-stream static pressure, lb/sq ft
P/P_0	static-pressure ratio
R	Reynolds number, based on capture area and free-stream conditions
RNI	Reynolds number index, $\delta/\psi\sqrt{\theta}$
$\dot{r}$	airplane yawing acceleration, radians/sec^2
S_1	location of fuselage static-pressure tap ahead of inlet
T	total temperature (assumed equal to free stream), $^{\circ}R$
t	time, sec
V_0	free-stream velocity, ft/sec
W_{by}	bypass air flow, lb/sec

H118

[redacted]

$\frac{W_{de}\sqrt{\theta}}{\delta}$	diffuser-exit corrected air flow, $\frac{\left(W_e + W_{by}\right)\sqrt{\theta}}{\delta}$, lb/sec
W_e	engine air flow, lb/sec
α	airplane angle of attack, deg
β	airplane corrected angle of sideslip, deg
δ	ratio of diffuser-exit total pressure to NASA sea-level standard pressure, $H_{de}/2116$
θ	ratio of diffuser-exit total temperature to NASA sea-level standard temperature, $T/518.4$
ρ_0	free-stream density, slugs/cu ft

$$\psi = \frac{735\ \theta^{1.5}}{T + 216}$$

AIRPLANE AND PROPULSION SYSTEM

The test airplane is a fighter type with a maximum speed capability of a Mach number of 2.0. Figure 1 presents a photograph of the airplane, and figure 2 shows a three-view drawing. Physical details are given in table I.

A pictorial view of the internal-flow system is shown in figure 3. Supersonic compression is achieved in each inlet by a conical shock generated by a 25° semiangle half cone. The inlet is designed for shock-cowl lip intersection at $M = 2.0$. The half cone is undercut from the apex to the inboard cowl section of the inlet for fuselage boundary-layer control (fig. 4). Cone-surface boundary layer is controlled at each inlet throat by means of a flush slot and is discharged through a sonic exit beneath the fuselage. Details of the cowl geometry and other pertinent diffuser information are also shown in figures 4(a) and (b). As seen in figure 3, the two ducts join a short distance ahead of the engine. For one of the flights discussed in this paper, a splitter plate was installed by the manufacturer at the end of the duct junction and extended approximately to the engine face (fig. 5). Also shown in this figure are the variable-position bypass doors which regulate the air flow around the engine for operation of the ejector nozzle and inlet mass-flow control.

[redacted]

The engine is of the axial-flow type with a 17-stage compressor. The first 6-stage stator vanes and the inlet guide vanes are varied as a function of corrected engine speed for surge suppression at part-speed operation. The exhaust nozzle is a variable-ejector type infinitely variable between minimum and maximum settings. The engine speed is held constant at the rated value of 7,460 rpm for the military setting and for the several afterburner throttle settings. The data of flight C of this paper were obtained after the engine manufacturer installed an automatic device to maintain rated engine speed during throttle reductions at flight speeds near $M = 2.0$.

INSTRUMENTATION

Induction-system pressure measurements were obtained at the engine compressor face, the left-inlet cone, and the left side of the fuselage. Figure 6 shows a photograph of the rake installation used to measure the total and static pressure of the air entering the engine. The rakes were installed radially at 60° intervals, and the total-pressure tubes were placed in the center of equal annular areas. Static-pressure orifices were installed in the accessory fairing at the same stations as the total-pressure tubes. Total and static pressure were measured also for the bypass air. The pressure orifices on the left-inlet cone, O_1 to O_5, and on the fuselage, S_1 and S_2, are detailed in figure 7. Most of the pressures were recorded on standard NASA 12-cell pressure recorders which had a reading accuracy of ±5 pounds per square foot. For the pressure system connected to the inlet cone, tests showed a flat-amplitude response to a sinusoidal input to 12 cycles per second. Several of the engine-face total pressures were sensed by temperature-compensated pressure transducers and were recorded on an oscillograph. Engine speed, stator-vane position, and compressor-discharge pressure were also measured, as was the engine plenum-chamber static pressure.

A standard NASA airspeed tube measured free-stream total and static pressure from a boom mounted on the airplane nose (fig. 1). Mach number is accurate to within ±0.01 for the airspeed range of this paper. Angle of attack and sideslip were also measured using vanes mounted on the boom. The airplane lateral motions used in this paper were recorded with standard NASA angular-velocity and angular-acceleration recorders. Free-stream total temperature was measured by a shielded resistance-type probe mounted on the fuselage.

All instruments were synchronized by a common timer.

[redacted]

TESTS, RESULTS, AND DISCUSSION

The tests reported in this paper were obtained at altitudes varying from about 42,000 feet to about 46,000 feet and at a Mach number of about 1.9. The airplane bypass area was kept at a nominal value of 82 square inches, the manufacturer's recommended setting for these speeds. Table II summarizes some pertinent parameters present at the onset of the nonsteady flow condition for each of the flights. It should be noted that the nonsteady flow occurred inadvertently for flight A, whereas in flights B and C the nonsteady flows were induced.

The test data are presented primarily in time-history form.

Flight A

Figure 8 presents the test data for flight A. Included are pertinent airplane parameters, a plot relating fuselage pressure ratio and airplane motion, induction-system parameters, and engine parameters. A left-roll maneuver was initiated at $t = 0.8$ second, as evidenced by the aileron-position records which are not shown in these data. The angle of sideslip shows a nose-right tendency after $t = 0.8$ second. Simultaneously, the yawing acceleration reversed a nose-right tendency and showed a nose-left tendency, as would be expected. Free-stream Mach number and angle of attack show somewhat steady values from $t = 0$ to at least $t = 2.0$ seconds. The engine parameters and the induction-system parameters, except for the system corrected air flow and mass-flow ratio and cone and fuselage pressures, also show steady values for this time interval. Figure 8(c) shows that the cone pressure O_1 agrees in trend but is somewhat less than that calculated by conical-shock theory (for example, ref. 3). Calculations are based on local Mach number ahead of the shock wave rather than free-stream Mach number. This condition will be seen for all data reported in this paper for an attached conical shock. A possible explanation of this result is a lower effective cone angle resulting from fuselage boundary-layer ingestion. The second cone pressure O_2 appears to bear a normal relation to O_1, but O_3 shows some evidence of expansion, which is possibly the result of a change in the nature of the compression-surface boundary layer during the roll. The normal shock is located between O_3 and O_4, as evidenced by the large increase in pressure between these two points. A large pressure increase is shown between O_4 and O_5. Since the diffuser geometric-area variation is negligible between these two points (fig. 4), it is believed that the throat bleed effectively increases the channel area thereby causing this compression. The plot of local recovery for the left and right engine face (fig. 8(d)) shows that the right face (uninstrumented cone)

[redacted]

exhibits recovery very close to two-shock recovery; whereas, the left face, corresponding to the instrumented side, shows a lower value for $t = 0$ to $t = 2.0$ seconds. Beginning at $t = 2.0$ seconds recovery drops markedly on the right side, indicating that the shock system on this side has begun to move forward, or upstream. This result has been observed in wind-tunnel studies of this configuration; specifically, during sideslip at reduced mass flow, the shock system moves forward on the leeward side past the inlet cone and forward on the fuselage. This condition is a consequence of twin-duct asymmetry. The sideslip angle has increased from a value of about 1.2° at $t = 2.0$ seconds to about 2.0° at $t = 2.6$ seconds, the maximum value of sideslip reached. At this time, several interconnected events occur. The left engine-face recovery shows a sharp increase toward a two-shock recovery. This phenomenon agrees with the analysis of reference 4. The cone pressures indicate a sharp increase in O_3 and O_2, indicating that the normal shock has moved forward of these points, but is still on the cone surface. The other diffuser parameters show a large decrease in value, except for distortion which shows a marked increase. Also, the pilot reported a loud bang and compressor surge; it was later verified that the engine flamed out. The plot of engine speed (fig. 8(e)) shows this result clearly. Approximately one second later the data show that the pilot quickly retarded throttle. The stator-vane record is seen to follow closely the pattern set by engine speed throughout the remainder of the data. The engine compartment pressure follows the pattern set by the left fuselage pressure for the remaining test data.

From figures 8(a) to 8(d), it is apparent that a periodic variation is present for the remainder of the test time. The extended duration of the motions and associated pressure changes is probably due to the low natural damping in yaw at the test conditions (ref. 5). From $t = 2.7$ seconds to $t = 3.4$ seconds the cone pressures show that the normal shock has moved downstream past O_3 and ahead of O_4 and remains at this point until $t = 4$ seconds, when the entire shock system moves forward past the cone to the side of the fuselage. This result is evidenced in a reduction in cone-surface pressures and an accompanying increase in fuselage pressures. For the remainder of the test data the shock system on the left inlet attaches and detaches in a periodic manner, producing periodic pressure changes as shown. A comparison of cone and fuselage pressures with airplane yawing acceleration (fig. 8(b), yaw damper off) shows a nose-right acceleration when the shock system detaches from the compression surface on the left side. This result is also obtained by comparing left and right engine-face-recovery data with airplane yawing acceleration. When the shock system detaches from the left side, a large decrease in recovery occurs at the left engine face. Large periodic decreases in pressure recovery are also evident on the right engine face, indicating a periodic shock-system detachment from the right-inlet cone as well as the left-inlet cone. Beginning at $t = 2$ seconds

[redacted]

it is seen (fig. 8(d)) that the shock system moves forward on the right side, as evidenced from the loss in recovery, but no large airplane motion is yet apparent. Therefore, it is concluded that the shock motion-airplane acceleration coupling was initiated by forward shock motion on the right side of the airplane.

The diffuser-exit parameters (fig. 8(f)) show large changes also, since these parameters represent a composite of the flow taking place in each of the ducts. It is noted that peaks in distortion coincide with peaks in sideslip angle.

Flight B

Nonsteady diffuser flow was obtained for flight B by means of an abrupt reduction in throttle. Table II summarizes the pertinent parameters present before the nonsteady flow occurred. It should be noted that the free-stream Mach number is essentially the same as that for flight A, but the distortion is considerably less. Figure 9 presents the same parameters as those plotted in figure 8 for flight A, with the addition of compressor pressure ratio. After an abrupt throttle reduction was initiated, at about $t = 3.0$ seconds, all the engine parameters (fig. 9(e)) show a decrease in value to the end of the test data. The diffuser exit (fig. 9(f)) and airplane parameters (fig. 9(a)) show reasonably steady values until $t = 3.7$ seconds. The cone pressures (fig. 9(c)) indicate the first cone pressure O_1 is slightly below the conical-shock-theory value, as discussed previously. Examination of the right and left engine-face recovery (fig. 9(d)) shows the right-side values to be near two-shock recovery prior to $t = 3.7$ seconds whereas the left side is operating above two-shock recovery to $t = 4.3$ seconds. This result may be due to multishock compression resulting from shock-boundary interaction, as mentioned in reference 2. Initial shock motion upstream occurs on the right side, as evidenced by a sharp drop in recovery on that side at some time after $t = 3.8$ seconds and continuing to $t = 7.3$ seconds where a value close to normal-shock recovery is reached. The cone-pressure data of figure 9(c) show that from $t = 3.7$ seconds to $t = 7.3$ seconds the normal shock moves from a position between O_3 and O_4 to a position downstream of O_4 with, apparently, a negligible effect on the local-pressure reading on the left side of the fuselage. Beginning at $t = 7.3$ seconds the shock system detaches on the left side and reattaches on the right side, as seen from the cone pressures and local engine-face pressures (figs. 9(c) and 9(d)). From this time to the end of the test, the shock systems alternately attach and detach in a periodic manner. During this nonsteady flow the normal shock is not located at the same point during the attached portion of the flow. For example, at $t = 10.3$ seconds the normal shock is located

[redacted]

between O_2 and O_3, whereas at t = 11.3 seconds the normal shock is located between O_3 and O_4.

A comparison of airplane yawing acceleration (fig. 9(b)) with that for flight A, shows much smaller excursions for flight B. This was probably due to yaw-damper activation in flight B. In addition, comparing local left- and right-side recoveries with normal-shock recoveries (fig. 9(d)) indicates that the detached shock system is probably not moving as far forward on the fuselage as for flight A (fig. 8(d)). Initial acceleration is a nose-left acceleration corresponding to shock detachment on the right side; this result agrees with flight A and wind-tunnel data. Initial shock detachment on the left cone results in a larger airplane acceleration than that which resulted from shock detachment on the right side. A decay in airplane acceleration is noted from about t = 11.2 seconds to the test limit for shock motions apparently similar to those obtained previous to this time.

The diffuser-exit parameters (fig. 9(f)) show large changes after t = 3.7 seconds which are comparable to those obtained for flight A.

Flight C

Nonsteady diffuser flow for flight C is shown in figure 10. For this flight a duct splitter plate was installed at the diffuser exit by the manufacturer. Prior to the nonsteady flow, the airplane had been placed in a directional-pulse maneuver with the yaw damper activated. Therefore, the yawing-acceleration trace (fig. 10(b)) shows periodic motion prior to any significant changes in cone pressures. Right and left engine-face recovery data show the two ducts to be operating at two-shock recovery prior to t = 1.0 second (fig. 10(d)). Initial shock motion occurs on the right side, as evidenced by a drop in right-face recovery at t = 1.0 second; the recovery at this time remains higher than normal-shock recovery, indicating an attached shock system on the right side. Since the airplane motion began prior to this shock motion, it is concluded that shock motion was initiated by the airplane motion because system mass flow was fairly constant. The cone pressures (fig. 10(c)) indicate the normal shock to be forward of O_3 for the attached system. The system detaches at about t = 1.6 seconds and about t = 3.0 seconds near the largest values of the nose-left attitude shown. The normal shock moves forward at t = 4.6 seconds and t = 6.2 seconds, but the shock system remains attached.

The airplane yawing acceleration (fig. 10(b)) shows a decay in directional motion to the test time limit. This result is compatible with the fact that the airplane yaw-damper system is operating and the shock-wave system does not move forward on the fuselage beyond t = 3.0 seconds.

Examination of the engine-performance parameters (fig. 10(e)) shows that the pilot executed an abrupt throttle reduction at about t = 2.5 seconds. The other engine parameters did not follow accordingly, since the engine rated speed was maintained by the automatic device mentioned in the AIRPLANE AND PROPULSION SYSTEM section; therefore, the throttle motion was ineffective in reducing the engine speed and air flow. Compressor pressure ratio, stator-vane position, and engine speed show consistent variations; engine-compartment-pressure variations follow the general trends of diffuser-exit recovery.

The test data of flight C are inconclusive regarding the effective- H
ness of the splitter plate in reducing the interaction phenomenon because 1
system mass flow was not reduced. However, pilot reports from similar 1
flights indicate a lessening of the interaction phenomenon and shock 8
audibility accompanying the shock motion during throttle reductions and directional maneuvers with the splitter plate installed. Thus, the splitter plate alleviated, but did not eliminate, the interaction phenomenon. No interaction phenomenon could be induced below a Mach number of about 1.8, with or without the splitter plate installed. Prior to installation of the splitter plate, pilot corrective action during the interaction phenomenon was to reduce throttle and increase angle of attack. This action would reduce airplane Mach number to less than M = 1.8.

CONCLUSIONS

Flight tests of a twin-duct propulsion system performed at a Mach number of about 1.9 during nonsteady propulsion-system operation have indicated the following conclusions:

1. An interaction occurs between airplane directional oscillation and fluctuation in an asymmetric inlet-shock configuration. The airplane directional motion could initiate the asymmetric shock configuration, or the asymmetric shock configuration could initiate the airplane directional motion.

2. The asymmetric inlet-shock configuration was produced at reduced mass flows and was aggravated by airplane sideslip angle. Initial forward motion of the inlet-shock system occurred on the leeward side of the airplane.

3. Installation of a duct splitter plate at the engine face alleviated, but did not eliminate, the interaction phenomenon. The use of a yaw damper was beneficial in reducing directional motions.

High-Speed Flight Station,
National Aeronautics and Space Administration,
Edwards, Calif., April 23, 1959.

REFERENCES

1. Obery, Leonard J., and Stitt, Leonard E.: Investigation at Mach Numbers 1.5 and 1.7 of Twin-Duct Side Air-Intake System With 9° Compression Ramp Including Modifications to Boundary-Layer-Removal Wedges and Effects of a Bypass System. NACA RM E53H04, 1953.

2. Stitt, Leonard E., McKevitt, Frank X., and Smith, Albert B.: Effect of Throat Bleed on the Supersonic Performance of a Half-Conical Side-Inlet System. NACA RM E55J07, 1956.

3. Dailey, Charles L., and Wood, Frank C.: Computation Curves for Compressible Fluid Problems. John Wiley & Sons, Inc., 1949.

4. Beke, Andrew: Criteria for Initial Flow Reversal in Symmetrical Twin-Intake Air-Induction Systems Operating at Supersonic Speeds. NACA RM E55L02a, 1956.

5. Andrews, William H., and Rediess, Herman A.: Flight-Determined Stability and Control Derivatives of a Supersonic Airplane With a Low-Aspect-Ratio Unswept Wing and a Tee-Tail. NASA MEMO 2-2-59H, 1959.

[redacted]

TABLE I

GEOMETRIC CHARACTERISTICS OF THE AIRPLANE

Wing:	
Airfoil section	Modified biconvex
Area, sq ft	196.1
Span, ft	21.94
Mean aerodynamic chord, ft	9.55
Root chord, ft	12.98
Tip chord, ft	4.89
Aspect ratio	2.45
Taper ratio	0.378
Sweep at 25-percent chord, deg	18.1
Sweep at the leading edge, deg	27.3
Incidence, deg	0
Dihedral, deg	-10.0
Airfoil thickness ratio	0.0336
Leading-edge flaps (per side) -	
Area, sq ft	8.50
Mean chord, ft	1.012
Deflection limit, deg	-30
Type	Plain
Trailing-edge flaps (per side) -	
Area, sq ft	11.55
Mean chord, ft	2.52
Deflection limit, deg	45
Type	Plain
Ailerons (per side) -	
Area, sq ft	4.73
Mean chord, ft	1.716
Span, ft	2.75
Deflection, deg	±15
Tail:	
Horizontal tail -	
Airfoil section	Modified biconvex
Area, sq ft	48.2
Mean aerodynamic chord, ft	4.415
Span, ft	11.92
Root chord, ft	6.16
Tip chord, ft	1.917
Aspect ratio	2.95
Taper ratio	0.311
Root thickness ratio	0.0493
Tip thickness ratio	0.0261

H118

[redacted]

TABLE I - Concluded

GEOMETRIC CHARACTERISTICS OF THE AIRPLANE

Tail length, 25-percent wing mean aerodynamic chord to 25-percent horizontal-tail mean aerodynamic chord, ft	18.72
Sweep at 25-percent mean aerodynamic chord, deg	10.12
Deflection limits, deg	5 to -17
Vertical tail -	
Airfoil section	Modified biconvex
Area, sq ft	35.1
Span, ft	5.46
Mean aerodynamic chord, ft	6.88
Aspect ratio	0.849
Taper ratio	0.371
Tail length, 25-percent wing mean aerodynamic chord to 25-percent vertical-tail mean aerodynamic chord, ft	15.13
Sweep at 25-percent mean aerodynamic chord, deg	35
Rudder -	
Area, sq ft	4.3
Span, ft	2.92
Average chord, ft	1.375
Deflection limit, deg	±25
Yaw damper -	
Area, sq ft	1
Span, ft	1
Average chord, ft	1
Deflection limit, deg	±20
Fuselage:	
Frontal area, sq ft	25
Length, ft	51.25
Fineness ratio	9.09
Dive brakes (per side):	
Area, sq ft (projected frontal area at maximum deflection)	4.13
Chord, ft	2.50
Deflection limit, deg	60
Weight:	
Empty weight, lb	13,237
Total take-off weight, lb	18,233
Center-of-gravity location, percent mean aerodynamic chord -	
Empty	17.40
Take-off	5.25

TABLE II

SUMMARY OF PERTINENT PARAMETERS PRIOR TO NONSTEADY FLOW

Flight	Maneuver	M_0	h_p, ft	RNI	$R \times 10^{-6}$	α, deg	β, deg	D, percent	Yaw damper	Remarks
A	Left roll	1.88	46,000	0.547	7.28	2.0	1.8	9.8	Off	Compressor surge and flameout, then pilot reduced throttle
B	Abrupt throttle reduction	1.86	43,900	.585	7.54	2.6	0	5.1	On	Nonsteady diffuser flow, no surge, induced by throttle
C	Directional pulse	1.93	41,600	.689	9.14	2.0	.8	7.9	On	Duct splitter plate installed. Nonsteady diffuser flow, no surge, induced by directional pulse, pilot reduced throttle

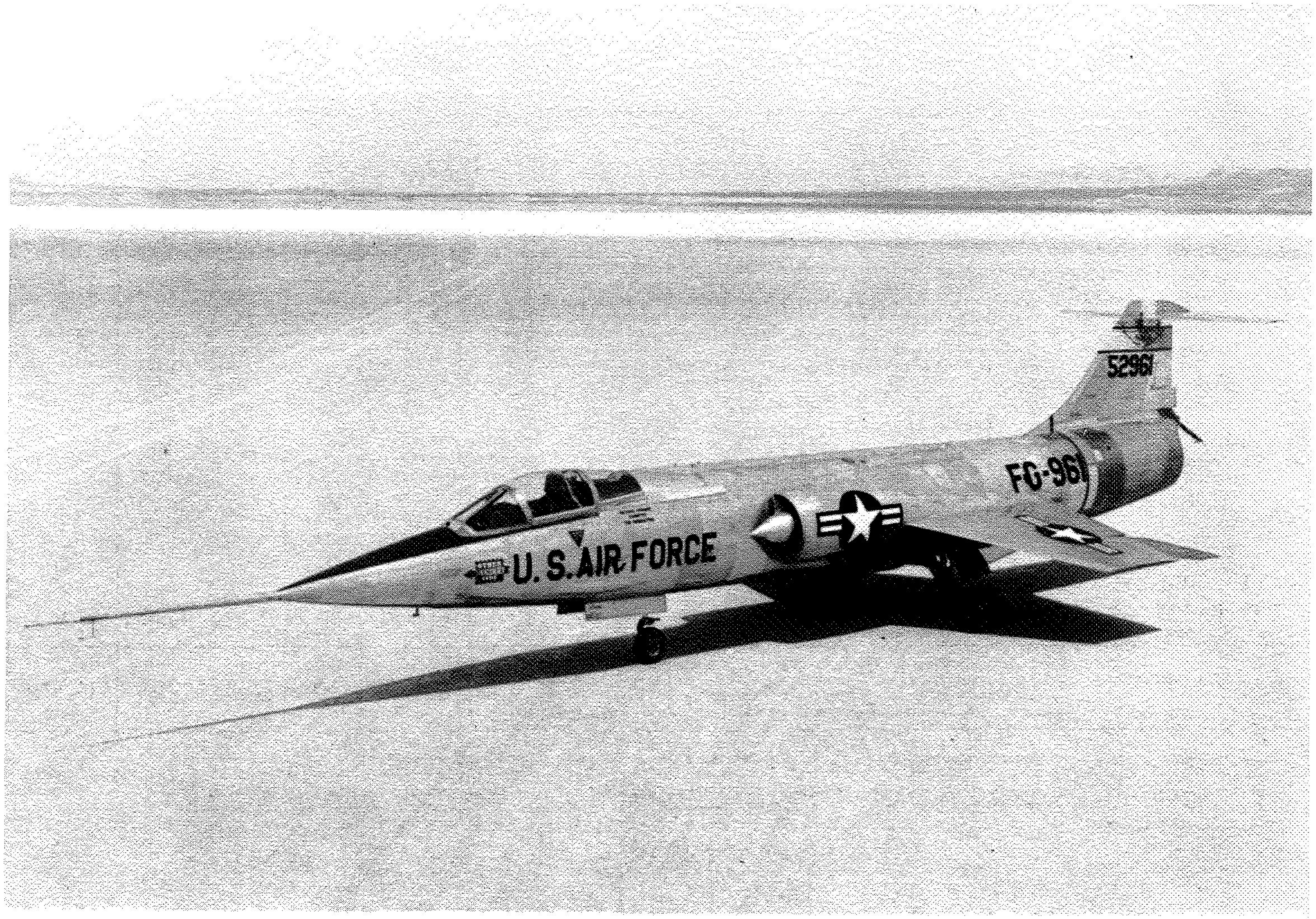
52961
FG-961
U. S. AIR FORCE

Figure 1.- Photograph of the test airplane. E-3022

[redacted]

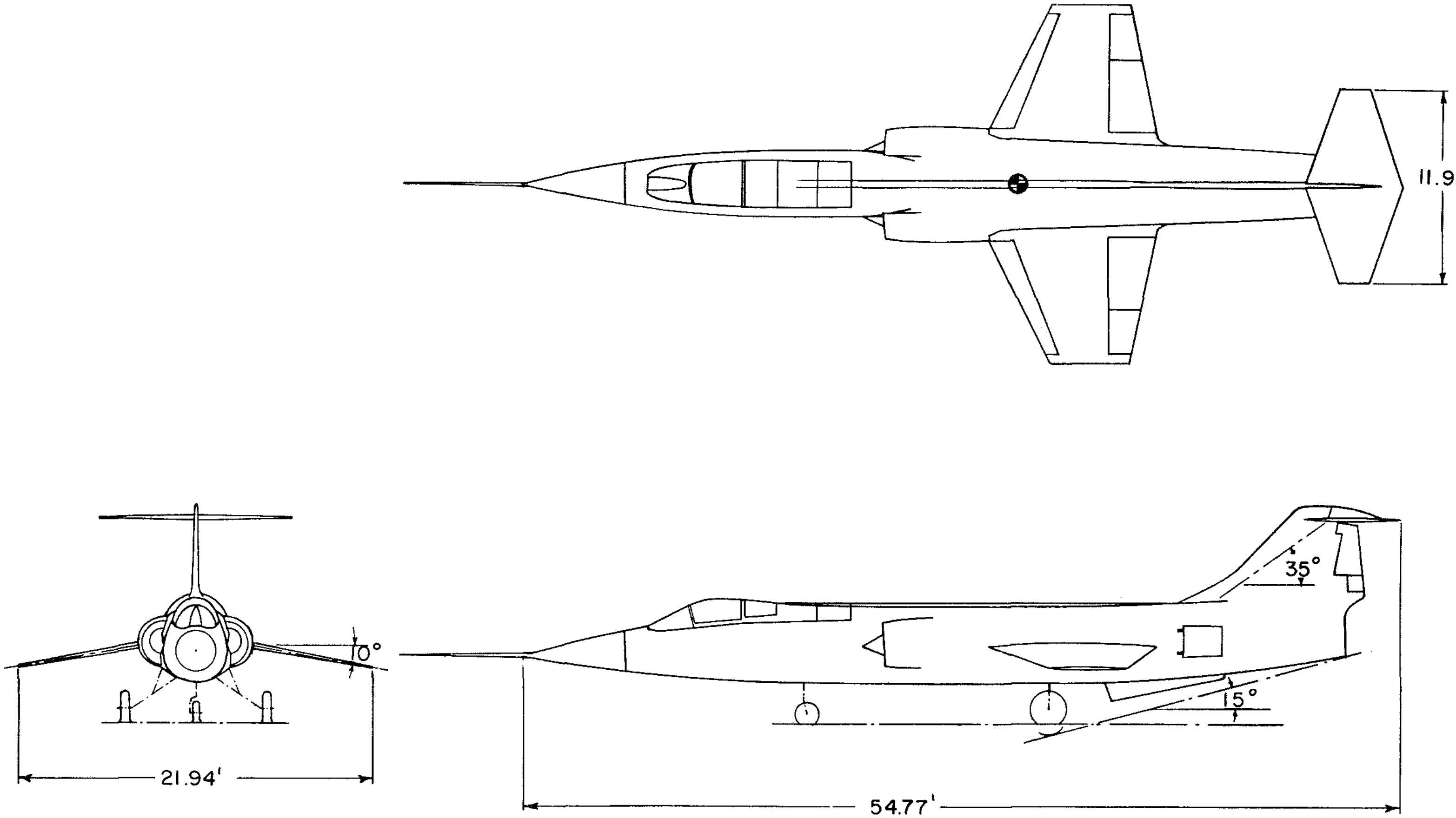
11.91'
35°
15°
0°
21.94'
54.77'

Figure 2.- Three-view drawing of the test airplane.

[redacted]

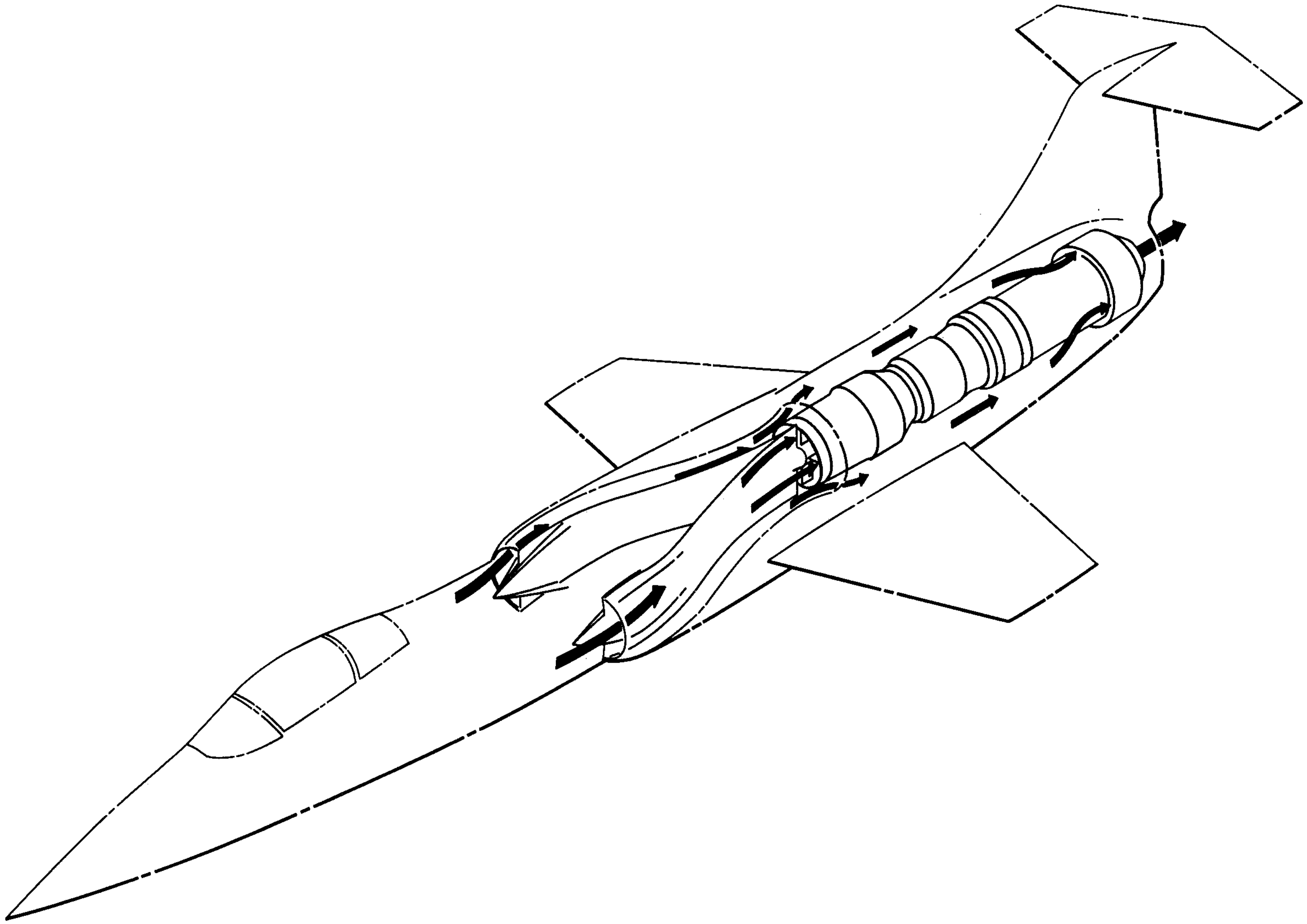

Figure 3.- Schematic drawing of internal-flow system.

[redacted]

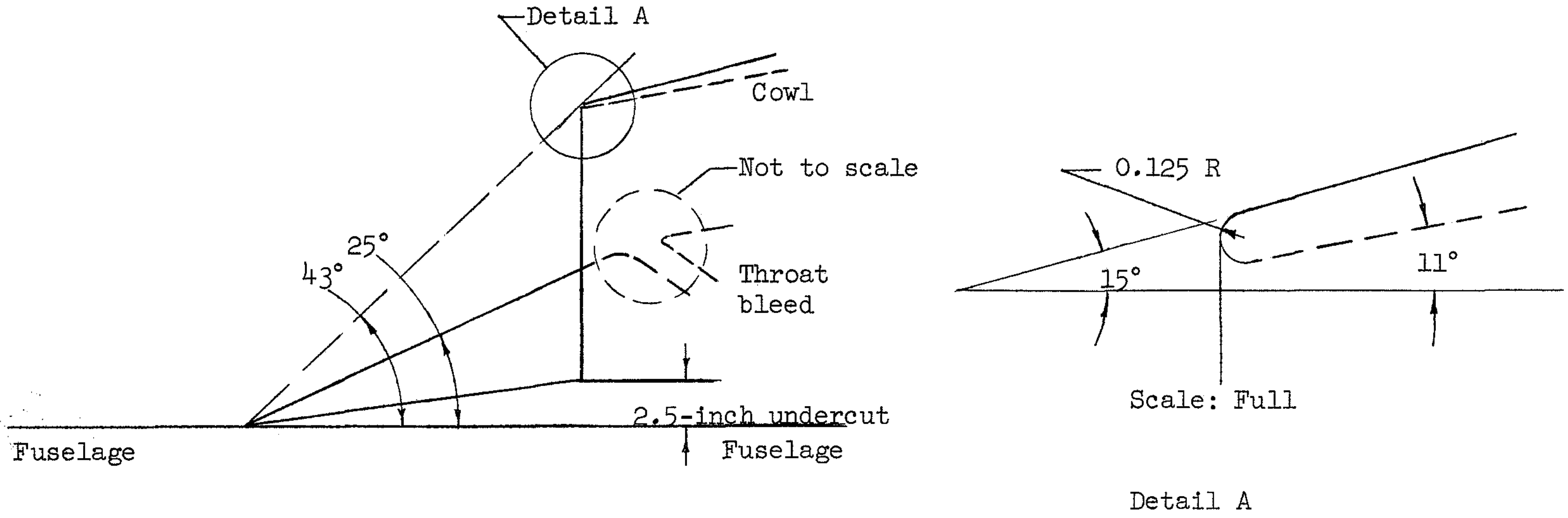
Detail A
Cowl
Not to scale
Throat
bleed
25°
43°
2.5-inch undercut
Fuselage
Fuselage
0.125 R
15°
11°
Scale: Full
Detail A

Scale: 0.1 in. = 1 in.

Capture area - 763 sq in. (both sides)

(a) Inlet details.

Figure 4.- Details of diffuser geometry.

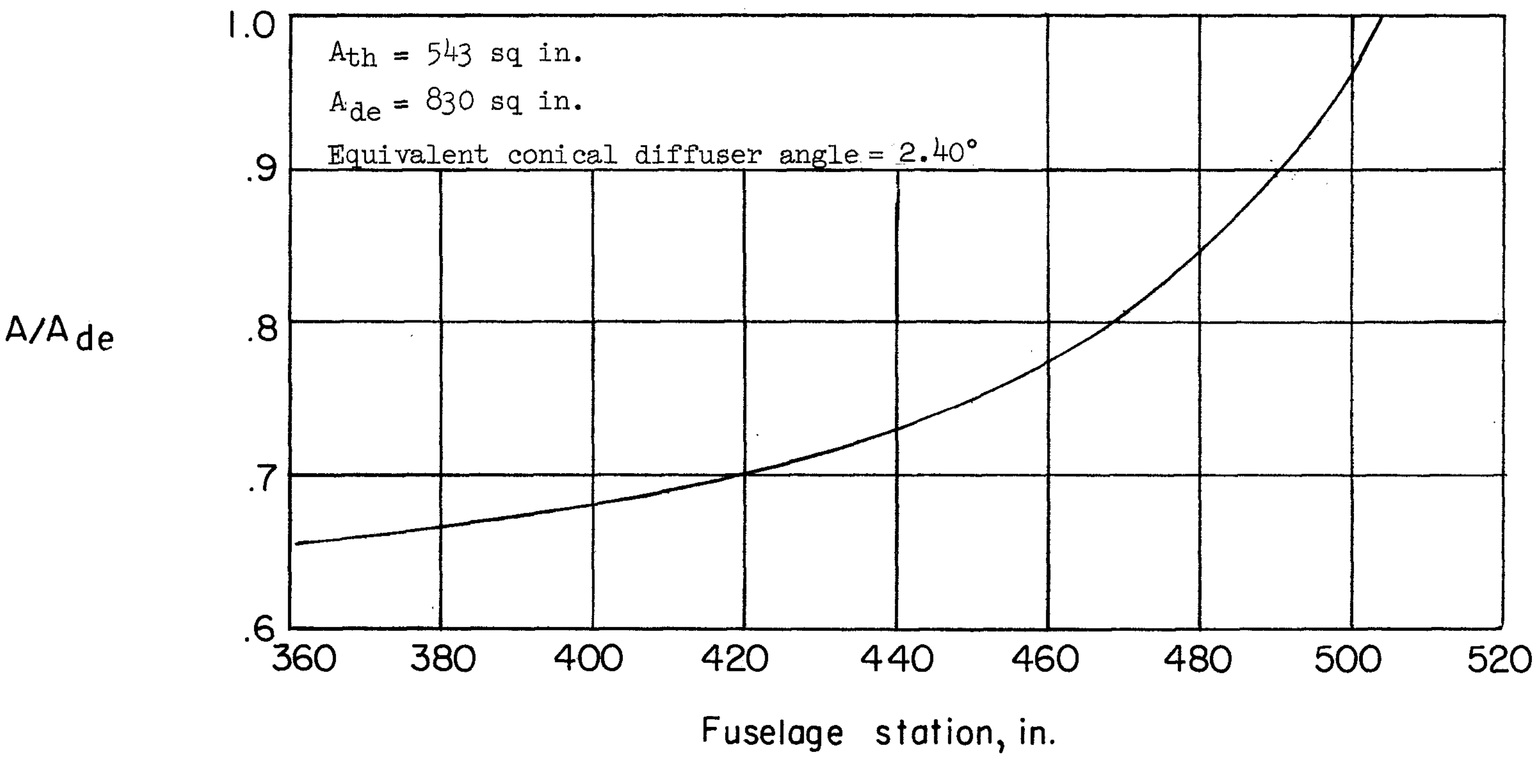

(b) Duct details.

Figure 4.- Concluded.

[redacted]

[redacted]

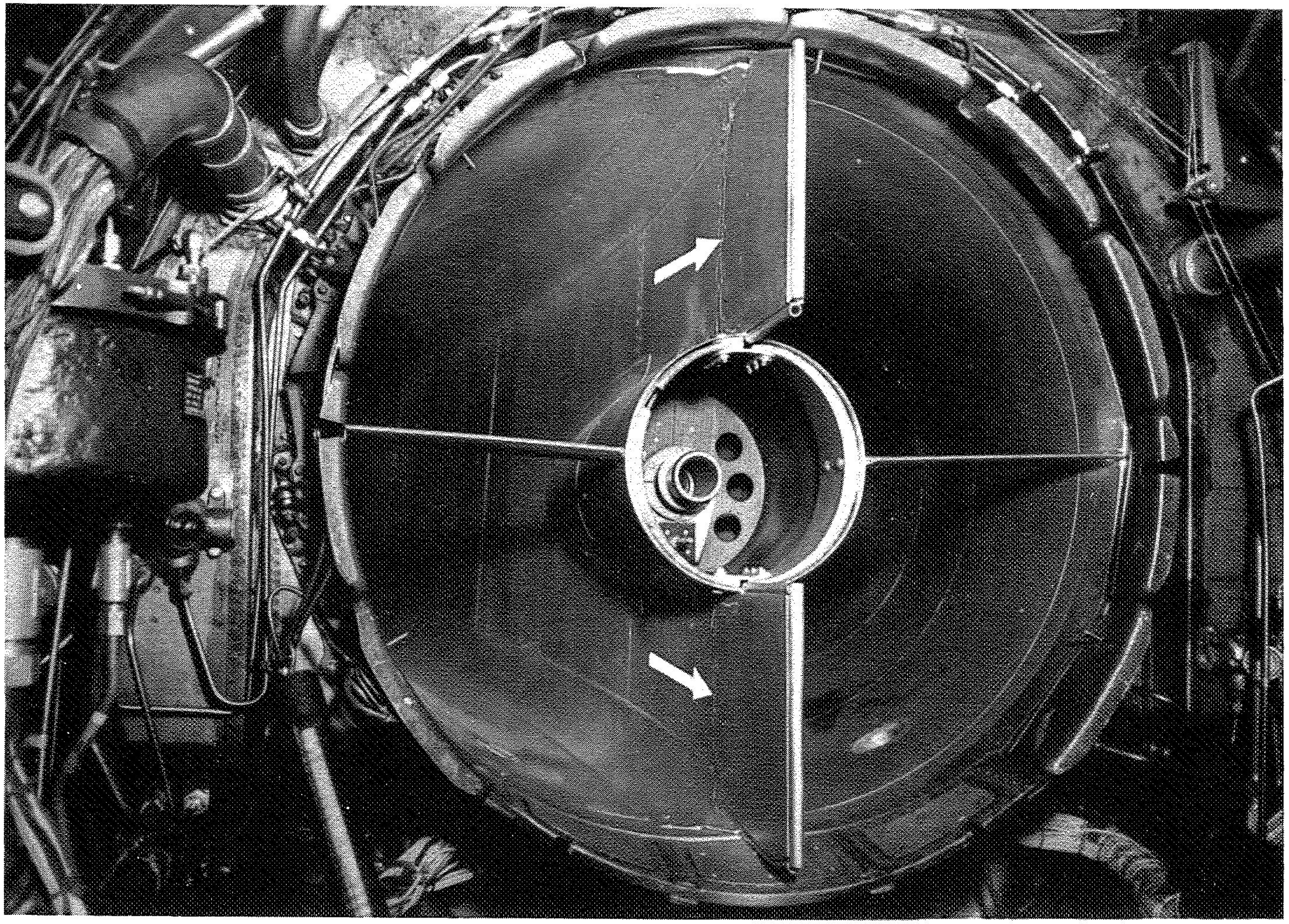

E-3104

Figure 5.- Photograph of splitter plate and supports installed at diffuser exit as indicated by arrows.

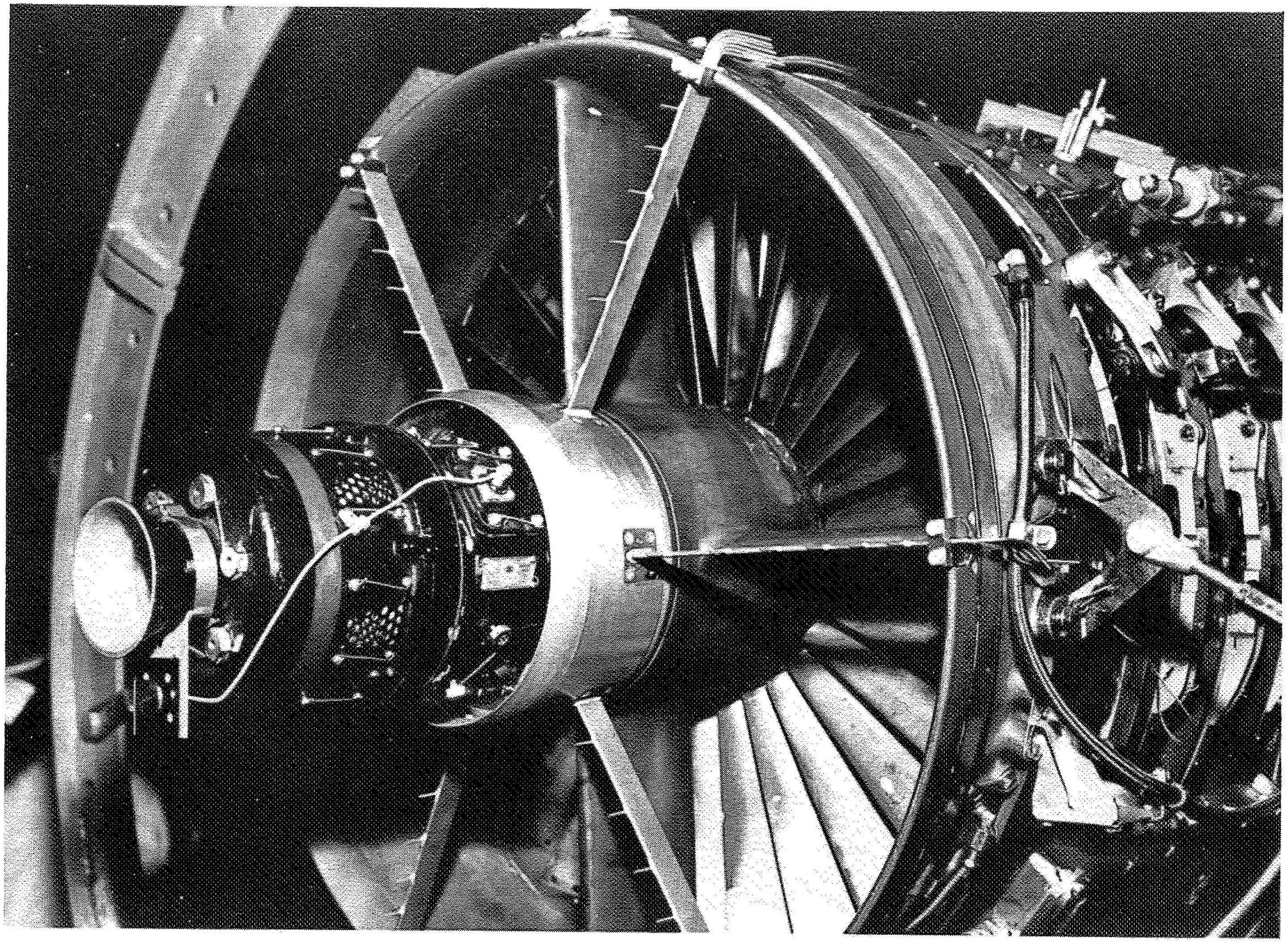

Figure 6.- Photograph of rake installation at engine-compressor face. Flow area equals 636 square inches. E-2661

[redacted]

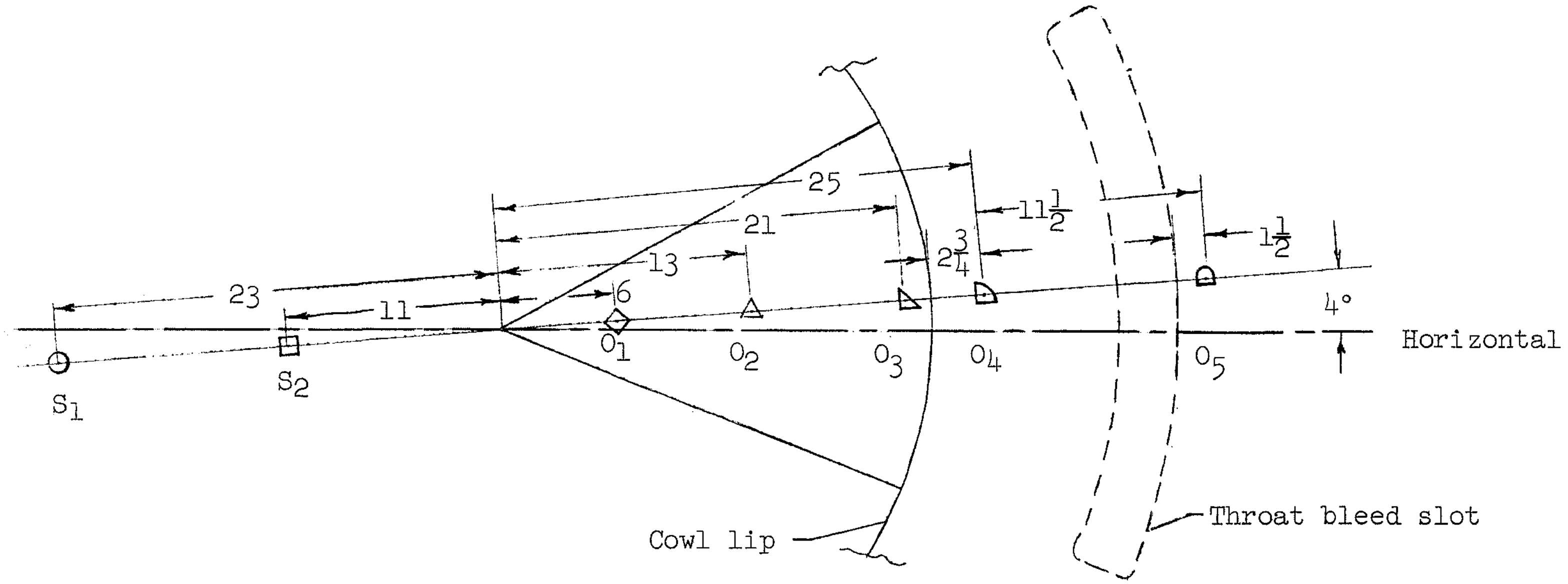
23
11
25
21
13
6
$2\frac{3}{4}$
$11\frac{1}{2}$
$1\frac{1}{2}$
4°
Horizontal
S_1
S_2
O_1
O_2
O_3
O_4
O_5
Cowl lip
Throat bleed slot

Scale: 0.1 in. = 1 in.

Figure 7.- Diagram of static-pressure orifices on and near the left-inlet cone. All dimensions in inches.

[redacted]

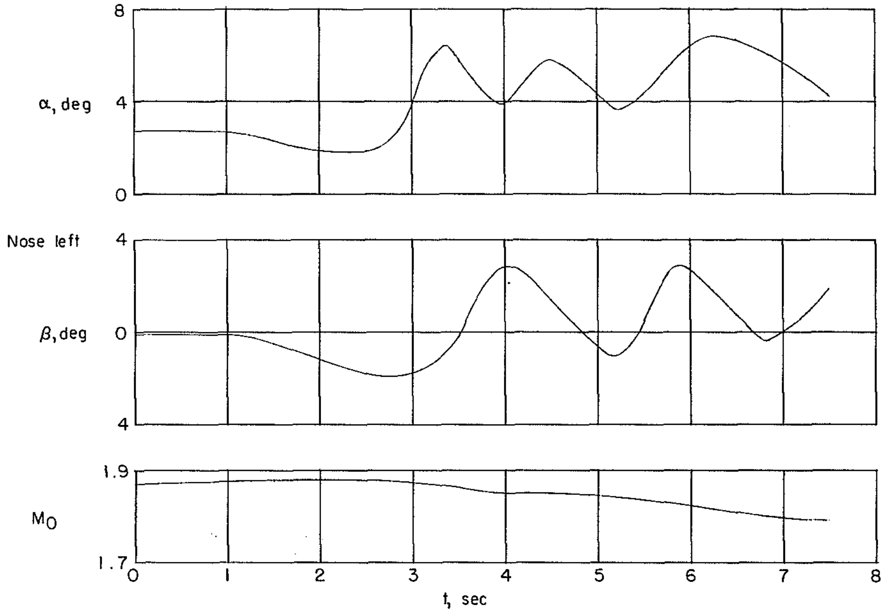

(a) Airplane parameters.

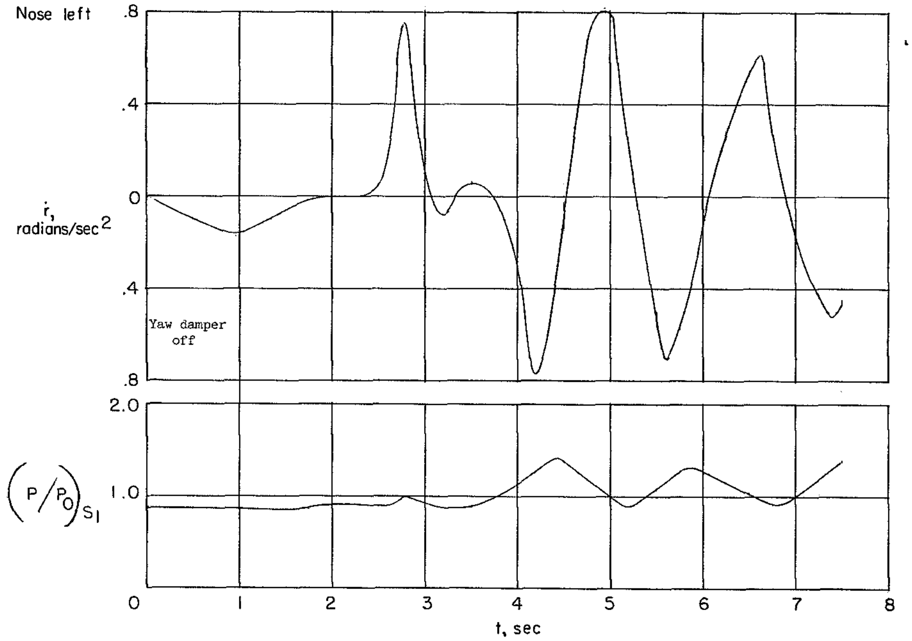

(b) Yawing acceleration and fuselage pressure ratio.

Figure 8.- Test data for nonsteady propulsion-system flow and airplane interaction induced by left roll.

[redacted]

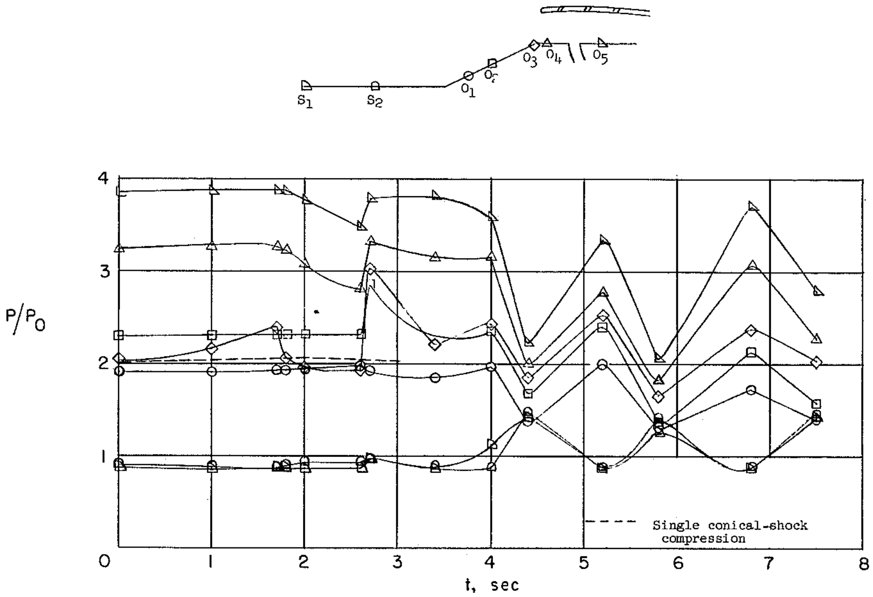

(c) Cone pressures.

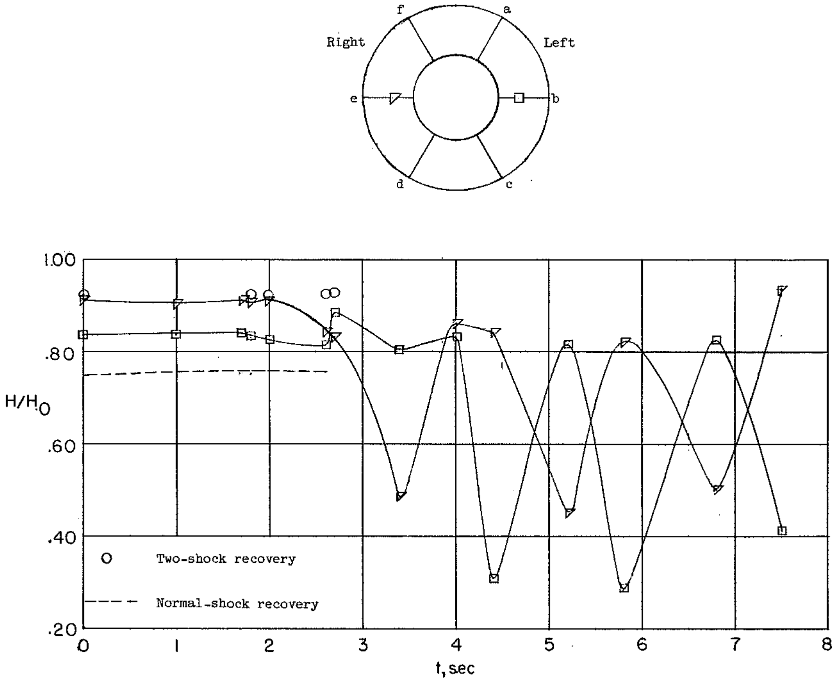

(d) Local engine-face recovery.

Figure 8.- Continued.

H-770

[redacted]

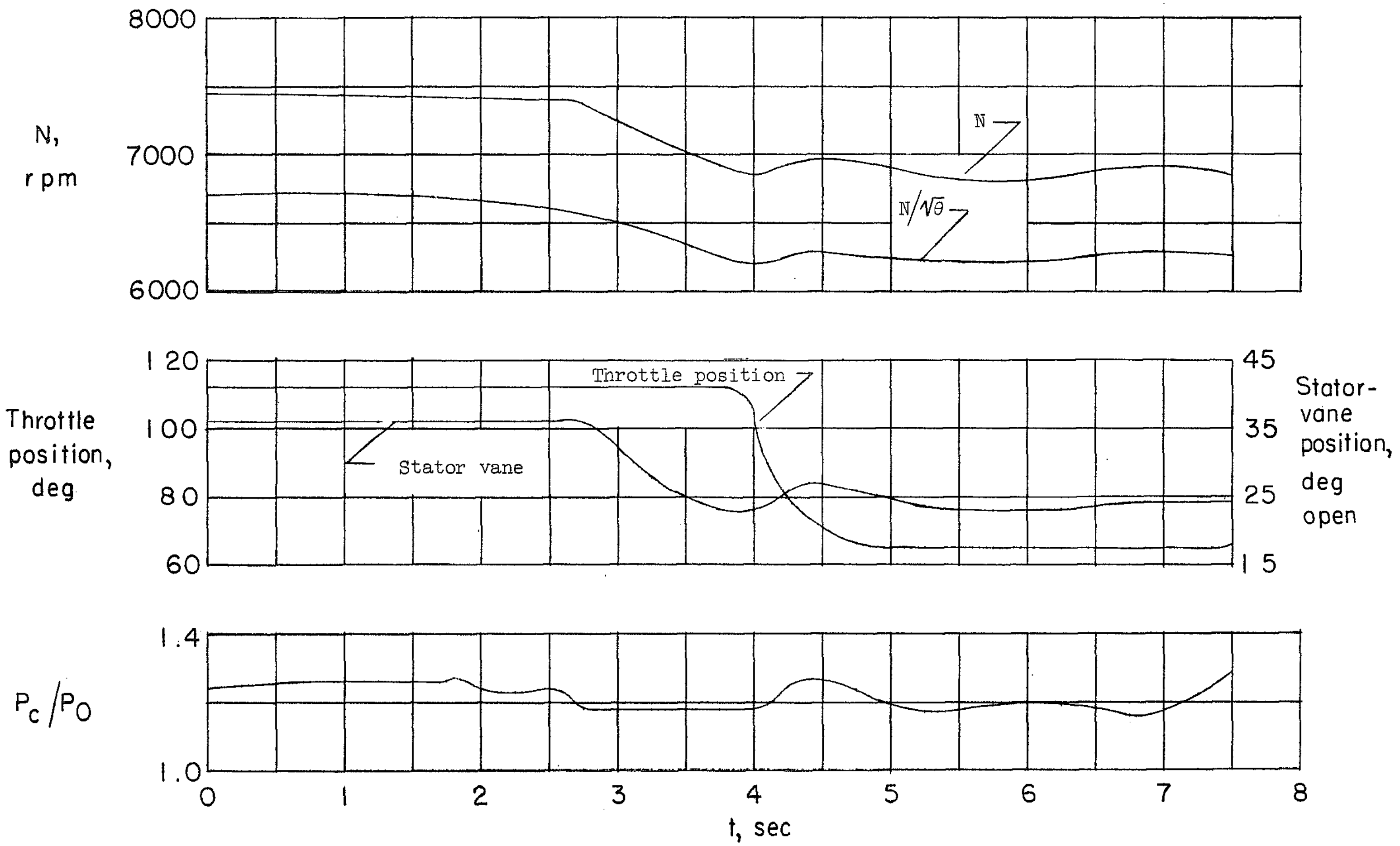

(e) Engine parameters.

Figure 8.- Continued.

[redacted]

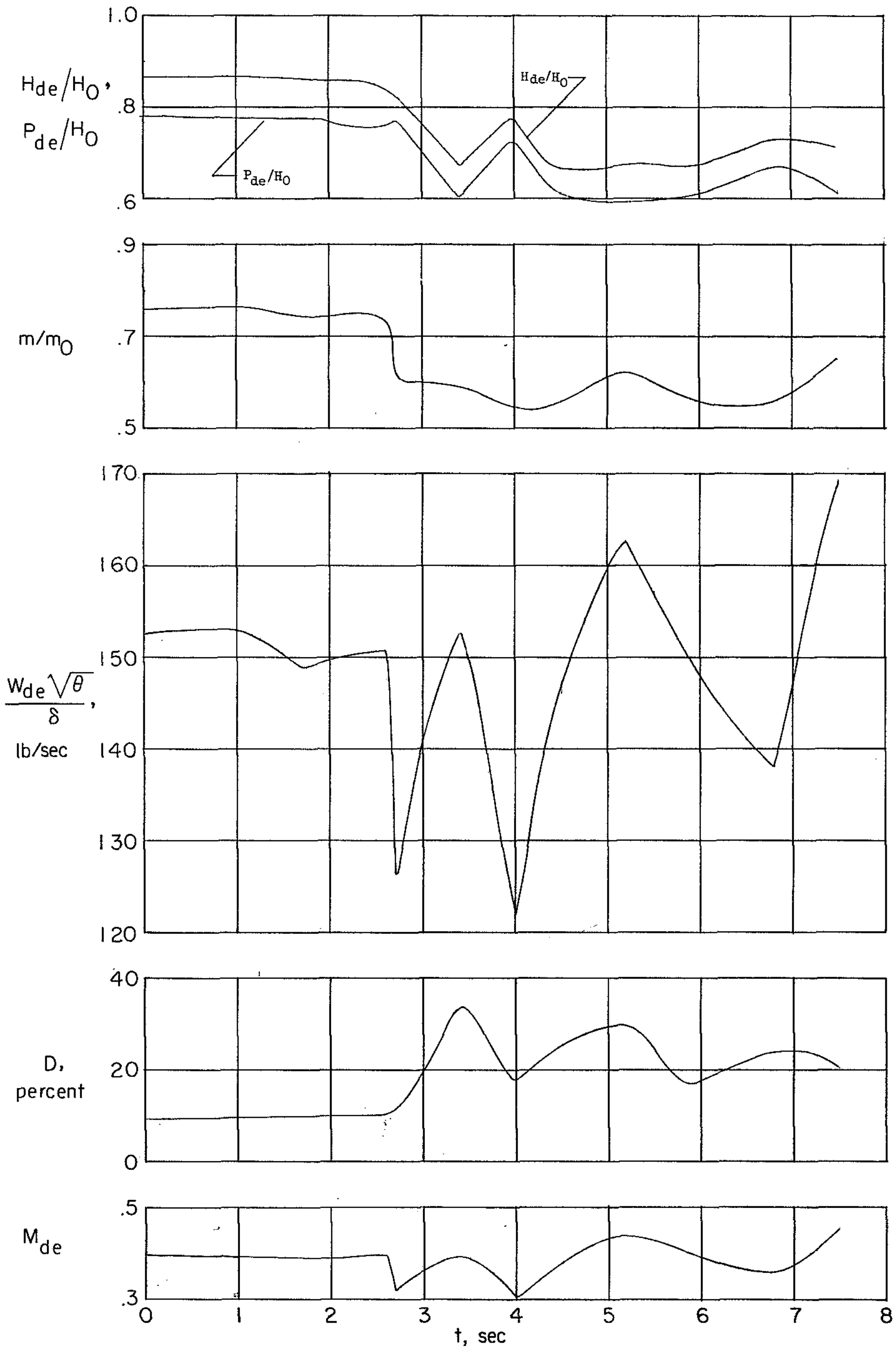

(f) Diffuser-exit parameters.

Figure 8.- Concluded.

H-118

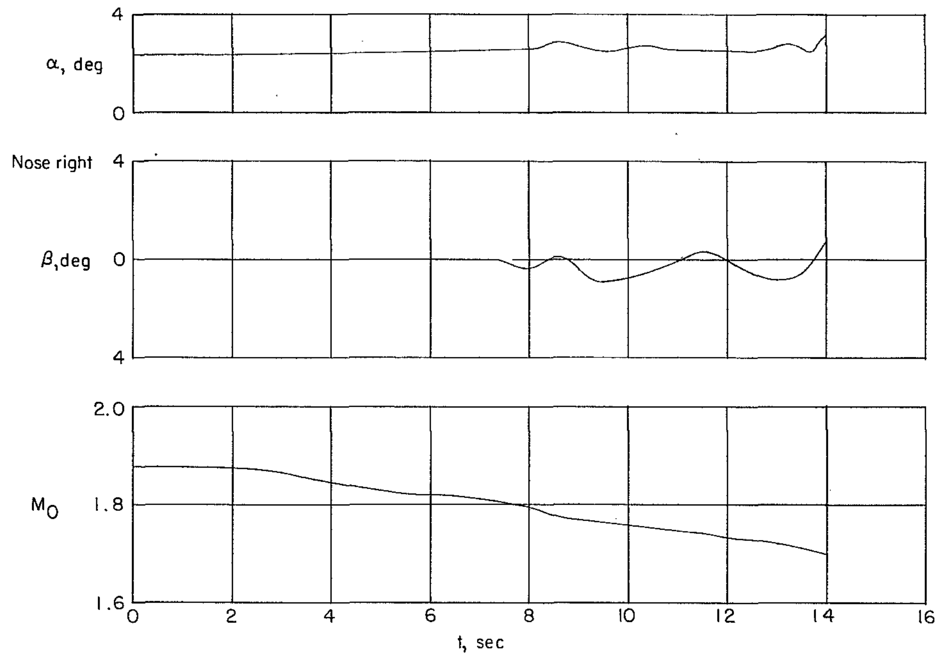

(a) Airplane parameters.

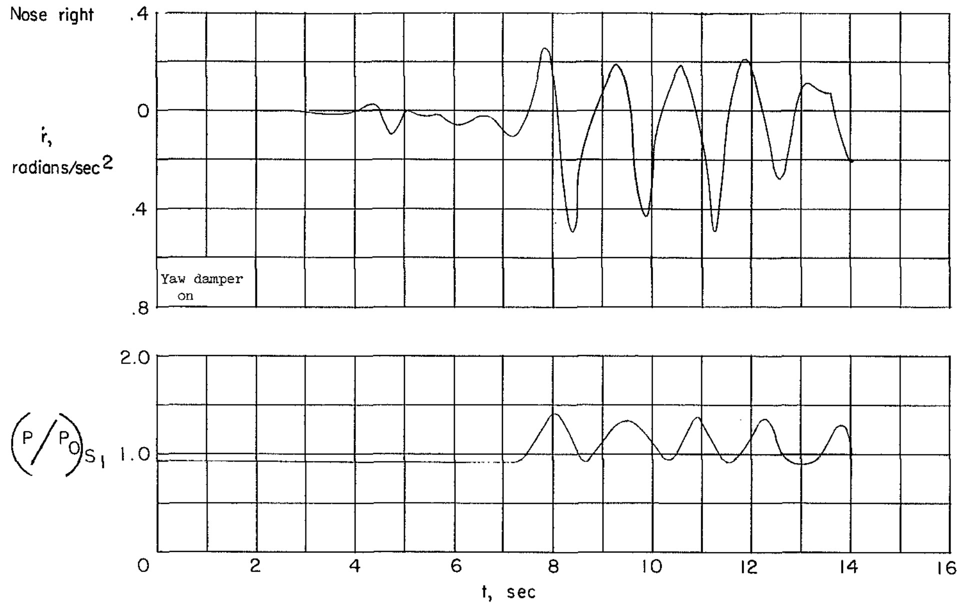

(b) Yawing acceleration and fuselage pressure ratio.

Figure 9.- Test data for nonsteady propulsion-system flow and airplane interaction induced by an abrupt throttle reduction.

[redacted]

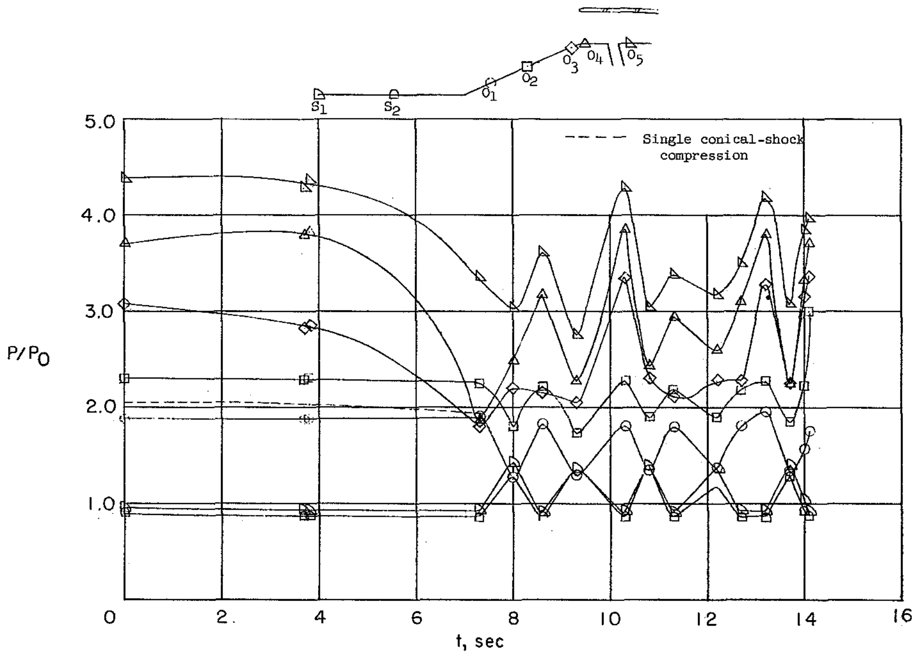

(c) Cone pressures.

H-118

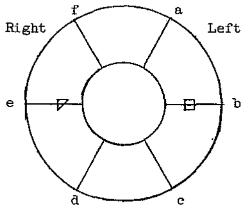
Right
f
a
Left
e
b
d
c

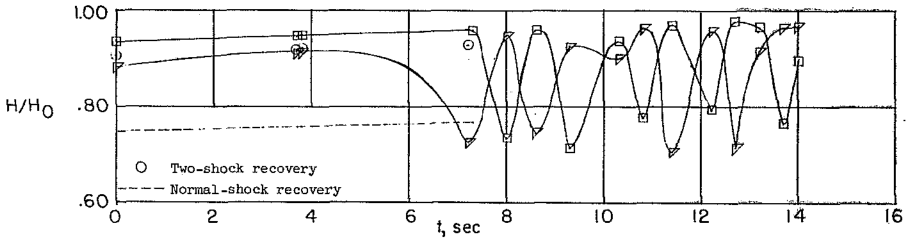

(d) Local engine-face parameters.

Figure 9.- Continued.

[redacted]

H-118

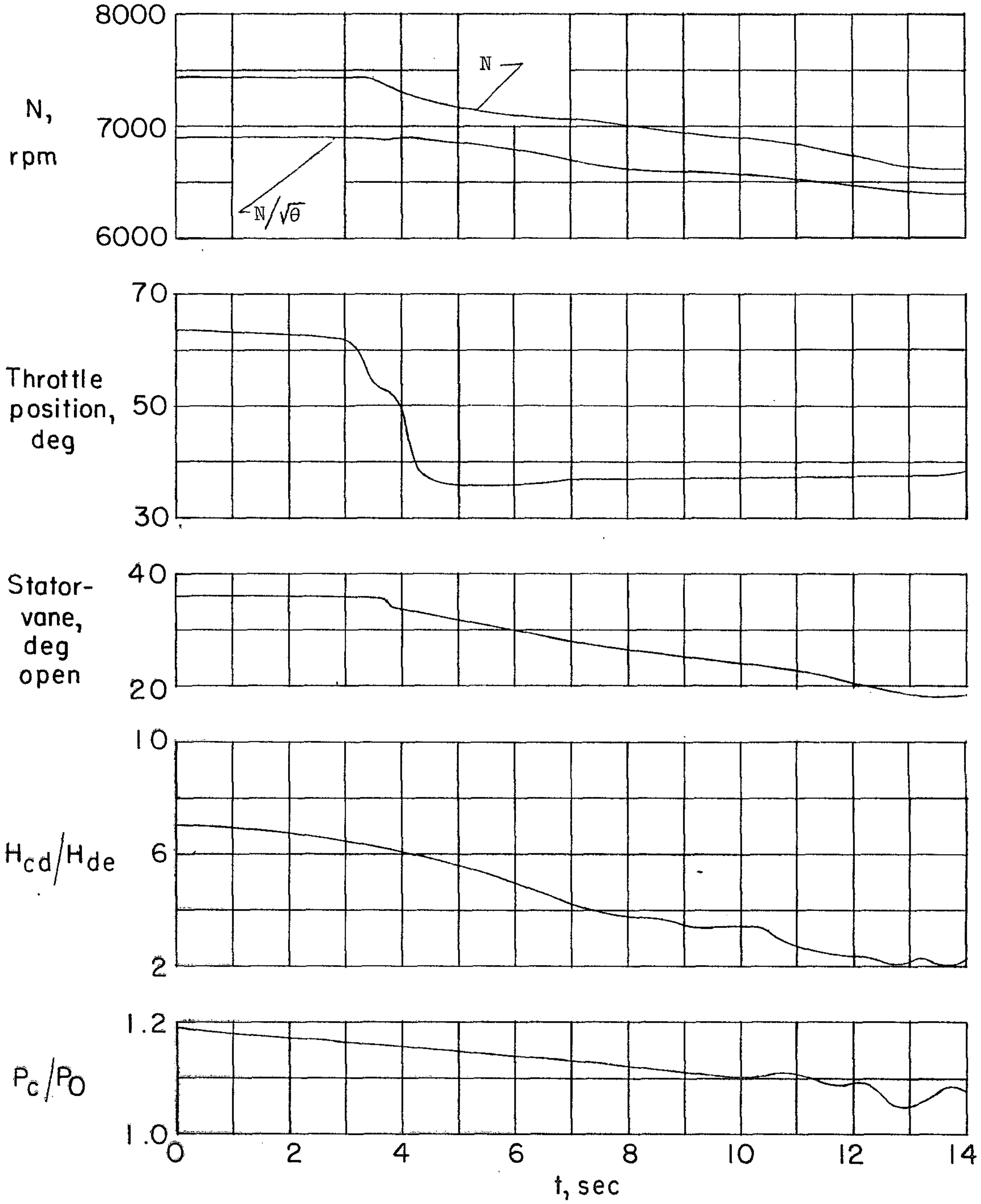

(e) Engine parameters.

Figure 9.- Continued.

[redacted]

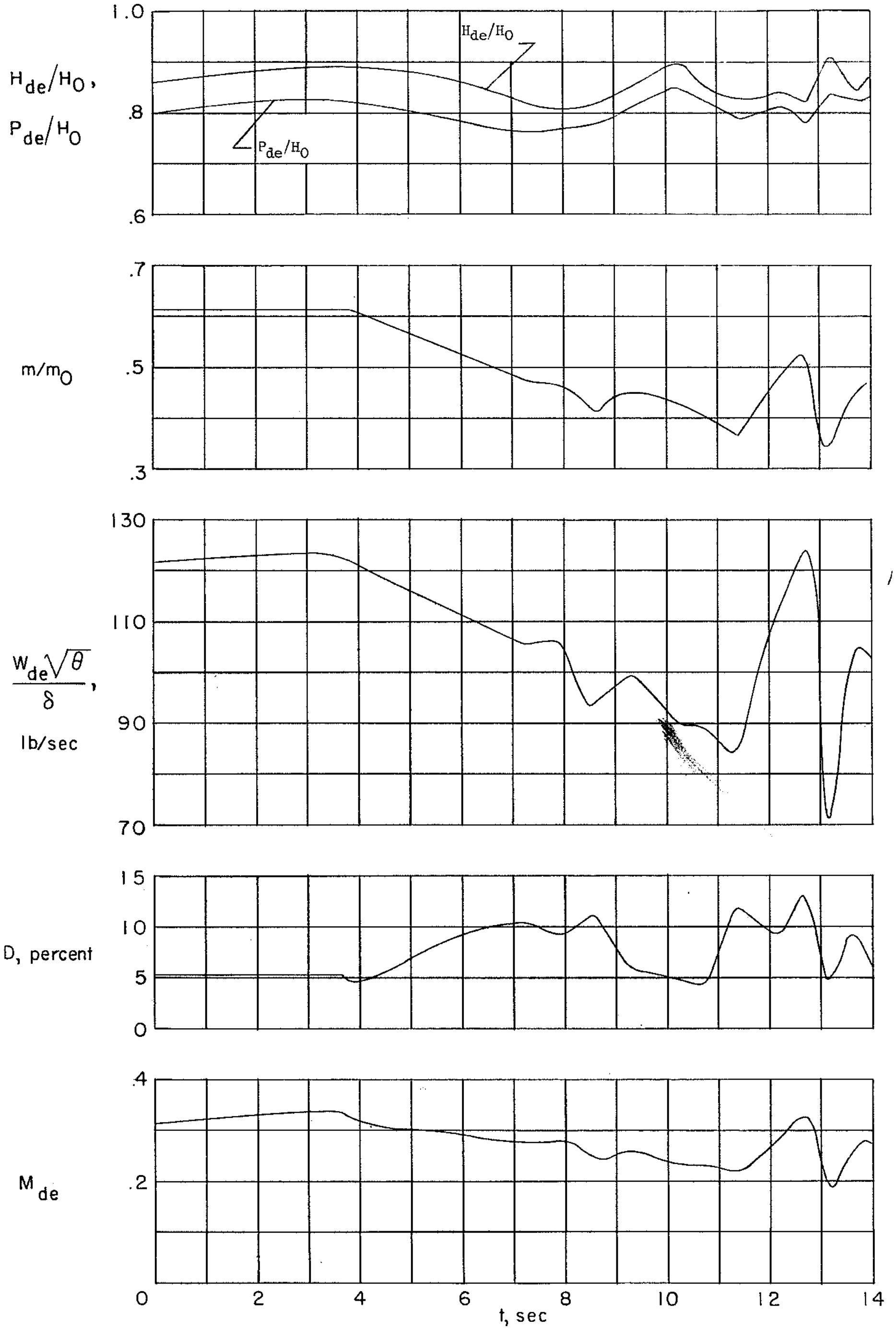

(f) Diffuser-exit parameters.

Figure 9.- Concluded.

H-110

[redacted]

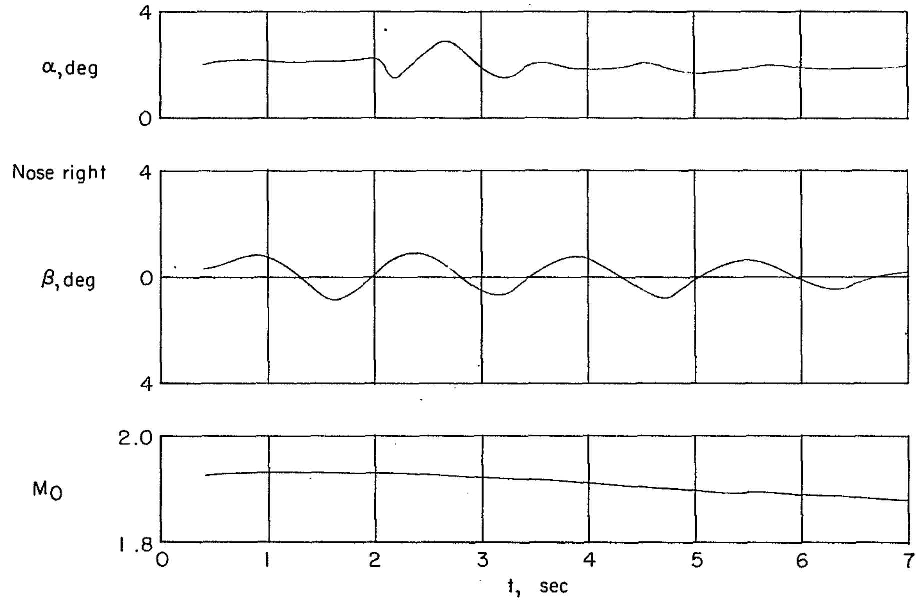

(a) Airplane parameters.

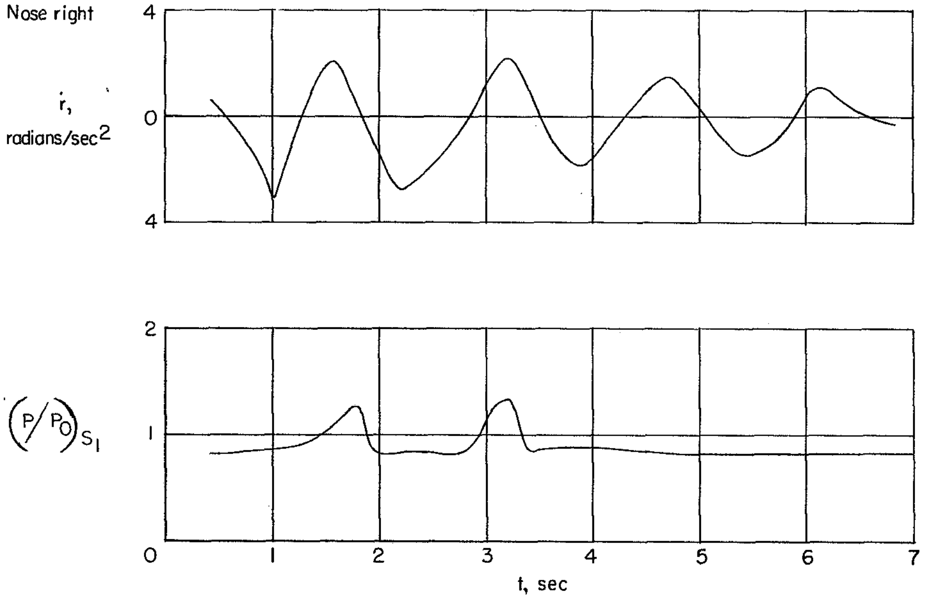

(b) Yawing acceleration and fuselage pressure ratio.

Figure 10.- Test data for nonsteady propulsion-system flow and airplane interaction induced by directional-pulse maneuver.

[redacted]

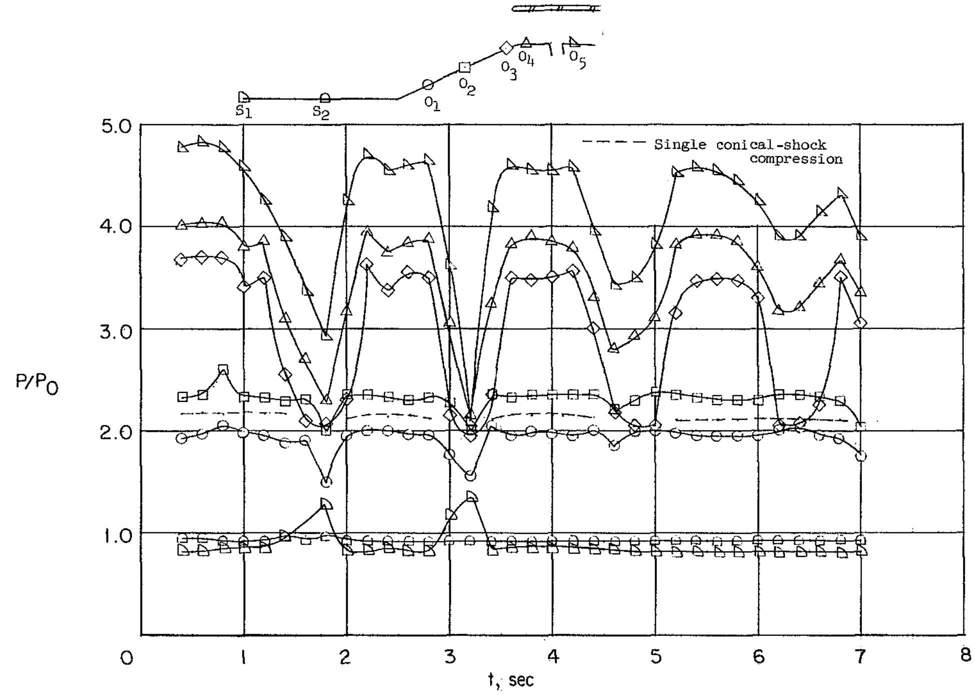

(c) Cone pressures.

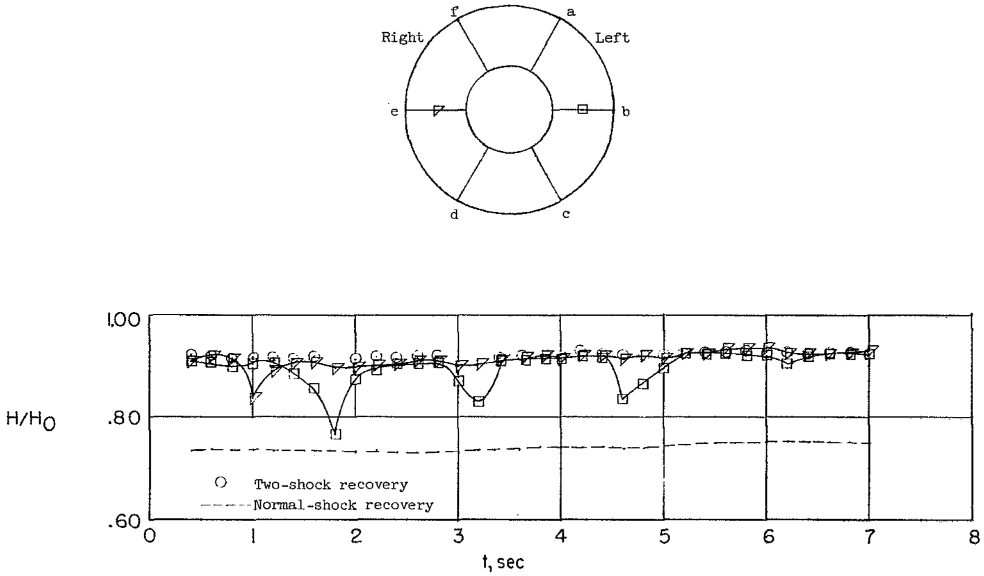

(d) Local engine-face recovery.

Figure 10.- Continued.

[redacted]

5Y

[redacted]

H-118

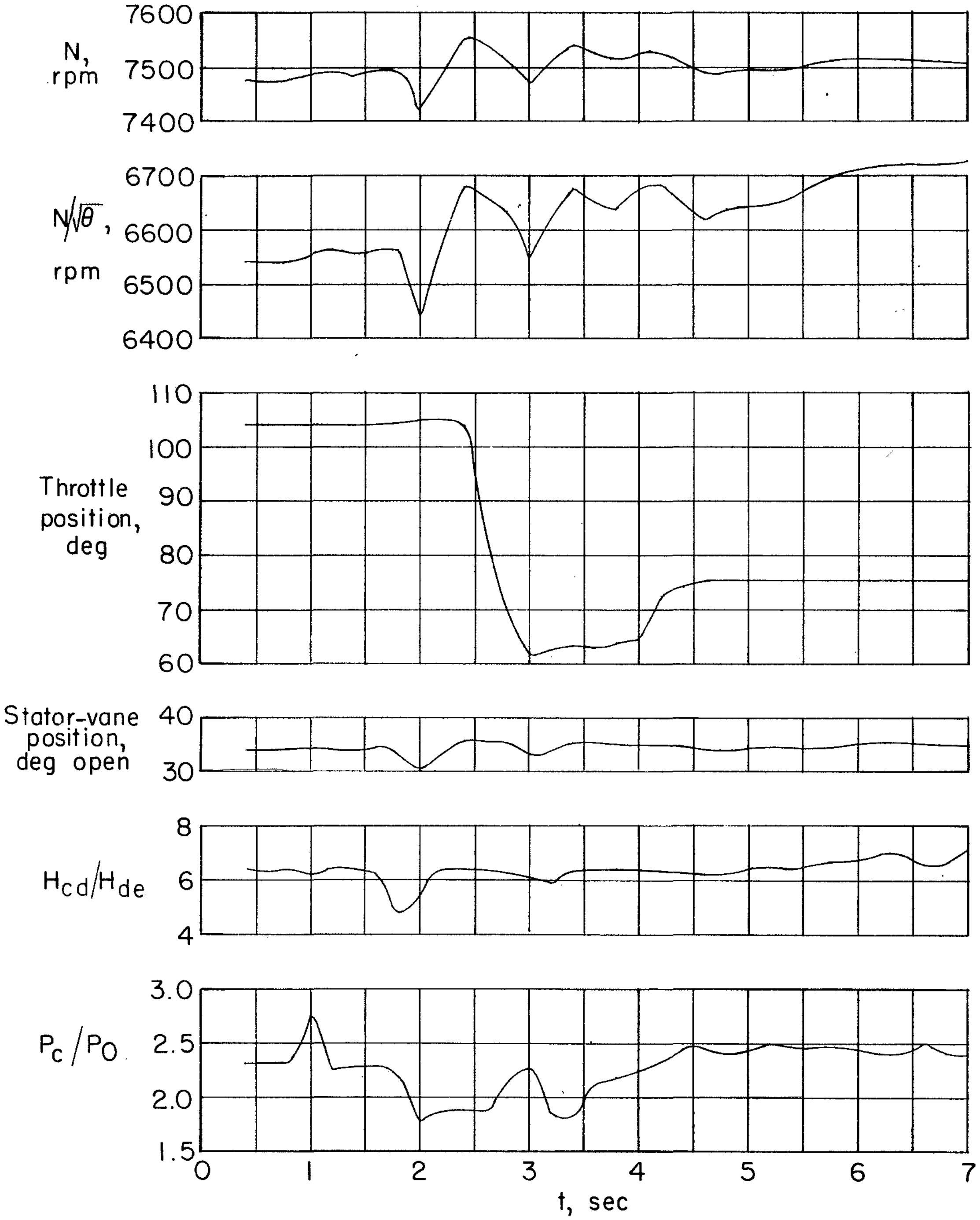

(e) Engine parameters.

Figure 10.- Continued.

[redacted]

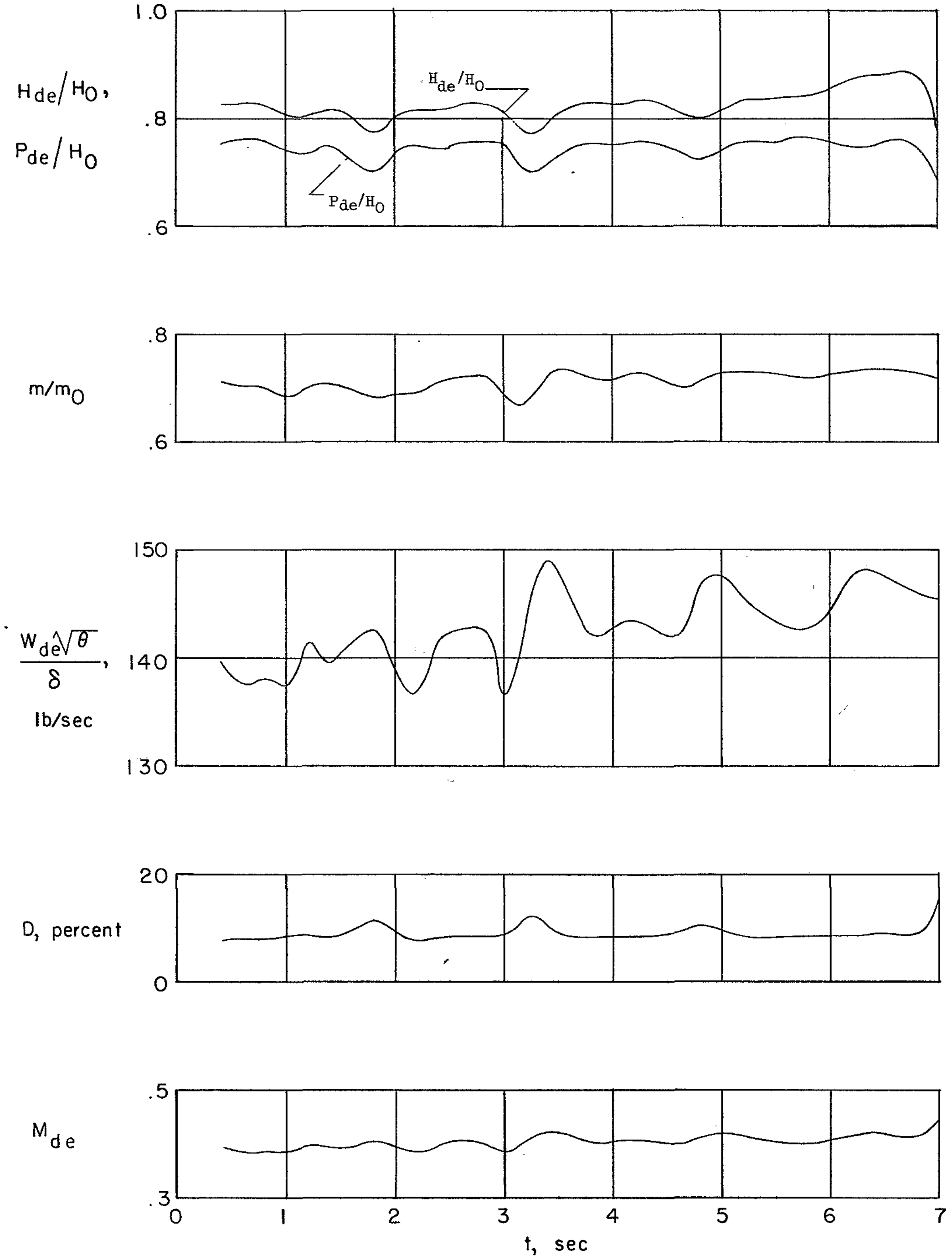

(f) Diffuser-exit parameters.

Figure 10.- Concluded.

H-118

[redacted]

NOTES: (1) Reynolds number is based on the diameter of a circle with the same area as that of the capture area of the inlet.

(2) The symbol * denotes the occurrence of buzz.

[redacted]

Report and facility	Description			Test parameters				Test data				Performance		Remarks
	Configuration	Number of oblique shocks	Type of boundary-layer control	Free-stream Mach number	Reynolds number $\times 10^{-6}$	Angle of attack, deg	Angle of yaw, deg	Drag	Inlet-flow profile	Discharge-flow profile	Flow picture	Maximum total-pressure recovery	Mass-flow ratio	
CONFID. NASA TM X-54 HSFS	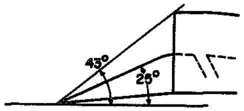	1	Cone undercut and flush slot at throat	1.86 to 1.93	7.28 to 9.14	1.8 to 6.4	0 to 1.8					0.91	0.34 to 0.76	Effect of duct splitter plate and sideslip on non-steady diffuser flow associated with airplane directional motions.
CONFID. NASA TM X-54 HSFS	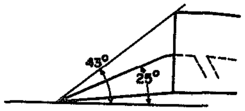	1	Cone undercut and flush slot at throat	1.86 to 1.93	7.28 to 9.14	1.8 to 6.4	0 to 1.8					0.91	0.34 to 0.76	Effect of duct splitter plate and sideslip on non-steady diffuser flow associated with airplane directional motions.
CONFID. NASA TM X-54 HSFS	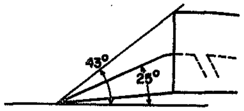	1	Cone undercut and flush slot at throat	1.86 to 1.93	7.28 to 9.14	1.8 to 6.4	0 to 1.8					0.91	0.34 to 0.76	Effect of duct splitter plate and sideslip on non-steady diffuser flow associated with airplane directional motions.
CONFID. NASA TM X-54 HSFS	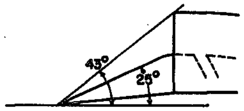	1	Cone undercut and flush slot at throat	1.86 to 1.93	7.28 to 9.14	1.8 to 6.4	0 to 1.8					0.91	0.34 to 0.76	Effect of duct splitter plate and sideslip on non-steady diffuser flow associated with airplane directional motions.

[redacted]

Bibliography

These strips are provided for the convenience of the reader and can be removed from this report to compile a bibliography of NASA inlet reports. This page is being added only to inlet reports and is on a trial basis.